Development of an approach for reliable GNSS positioning under presence of local ionospheric disturbances

Kinga Wężka [1], Marija Cokrlic [1], Roman Galas [1], Norbert Jakowski [2], Volker Wilken[2]

[1]Institute of Geodesy and Geoinformation Science, Technical University of Berlin
[2]Institute of Communications and Navigation, German Aerospace Centre

IAG-C.4 2016, September 4-7, 2016, Wrocław, Poland

Motivation

Global and regional ionospheric models are provided
and some of them will be available (e.g. SWACI) even in real-time.
Nevertheless
monitoring of local (small scale) state of the ionosphere
for accurate and reliable GNSS positioning might be required to reduce degradation of the PVT solutions
which can be caused by ionospheric irregularities.

For example: Estimation of parameters expressing local ionospheric irregularities (perturbations), on-the-site, might help to reduce degradation of the PVT solutions.

*) SWACI model (DLR) will provide TEC maps with 10 min delay and 2.5°x 5.0° resolution in space.

Motivation

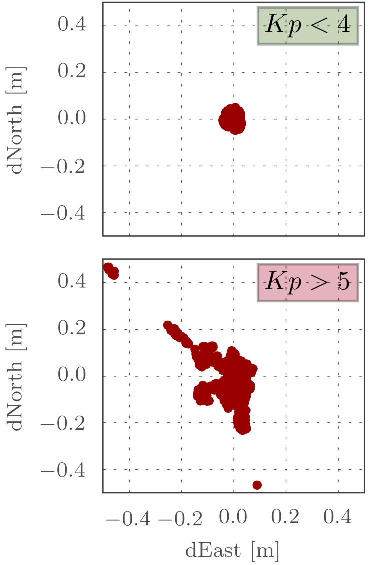

Problem Statment

- Low spatial and temporal resolution of available ionospheric products
- Lack of information about the local ionospheric irregularities

Impact on GNSS observables

- The ionospheric disturbances cause significant **degradation in the accuracy and reliability** of GNSS observables
- Their impact on GNSS observations can cause: **higher noise level of GNSS signal, cycle slips, outlier observations (blunders) and loss of signal lock**

Outline of the Presentation

Single station monitoring of the local state of the ionosphere

The following parameters are estimated :

- Slant Total Electron Content ($sTEC$),
- Rate of TEC (ROT), and Rate of TEC index ($ROTI$),
- Amplitude scintillation indices ($S4$);
- Carrier phase scintillation indices (σ_ϕ)

Aplicability of ionospheric parameters

- To reduce impact of ionospheric effect on GNSS observable
- To define the stochastic model of GNSS observations
- Receiver Autonomous Integrity Monitoring for detection and isolation of a faulty observable

IONO-Tools output

Technical University of Berlin

Flow diagram of the TUB-software for estimation ionospheric parameters

C, C++, PYTHON

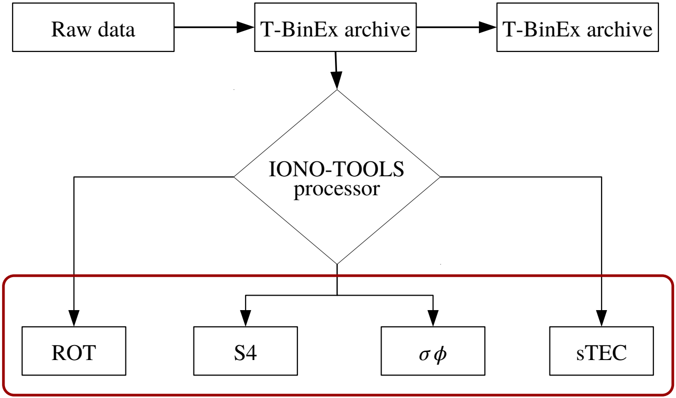

Processor for on-site estimation of the sTEC

Technical University of Berlin

The processor estimates slants TEC from code- and carrier phase observations using the so called "LEVELLING APPROACH"

$$sTEC^s_{g,R}(t_j) = B' \left(\frac{1}{c} P^s_{GF,R} - DCB^s_{f1-f2} - DCB^s_{f1-f2,R} \right)$$

$$sTEC^s_{ph,R}(t_j) = B' \left(\frac{1}{c} P^s_{GF,R} - DPB^s_{f1-f2} - DPB^s_{f1-f2,R} \right) - \frac{1}{c} \lambda_{GF} N^s_{GF,R}$$

$P^s_{GF,R}, L^s_{GF,R}$	:	geometry free code- and carrier phase observables,
$DCB^s_{f1-f2}, DCB^s_{f1-f2,R}$	:	between the frequencies satellite- and receiver hardware delays of the code phase observations,
$DPB^s_{f1-f2}, DPB^s_{f1-f2,R}$	:	between the frequencies satellite- and receiver hardware delays of the carrier phase observations

Converts calculated GF combination from meters to TECU (TEC units)

$$B' = \frac{1}{40.3} \frac{f_1^2 f_2^2}{f_1^2 - f_2^2}$$

Processor for on-site estimation of the sTEC

Technical University of Berlin

The processor estimates slants TEC from code- and carrier phase observations using the so called "LEVELLING APPROACH"

$$sTEC^{s}_{g,R}(t_j) = B' \left(\frac{1}{c} P^{s}_{GF,R} - DCB^{s}_{f1-f2} - DCB^{s}_{f1-f2,R} \right)$$

$$sTEC^{s}_{ph,R}(t_j) = B' \left(\frac{1}{c} P^{s}_{GF,R} - DPB^{s}_{f1-f2} - DPB^{s}_{f1-f2,R} \right) - \frac{1}{c} \lambda_{GF} N^{s}_{GF,R}$$

$P^{s}_{GF,R}, L^{s}_{GF,R}$	:	geometry free code- and carrier phase observables,
$DCB^{s}_{f1-f2}, DCB^{s}_{f1-f2,R}$	:	between the frequencies satellite- and receiver hardware delays of the code phase observations,
$DPB^{s}_{f1-f2}, DPB^{s}_{f1-f2,R}$	:	between the frequencies satellite- and receiver hardware delays of the carrier phase observations

Converts calculated GF combination from meters to TECU (TEC units)

$$B' = \frac{1}{40.3} \frac{f_1^2 f_2^2}{f_1^2 - f_2^2}$$

GPS receiver inter-frequency biases must be calibrated!

Levelling of carrier-phase by code-phase

DLR
Technical University of Berlin

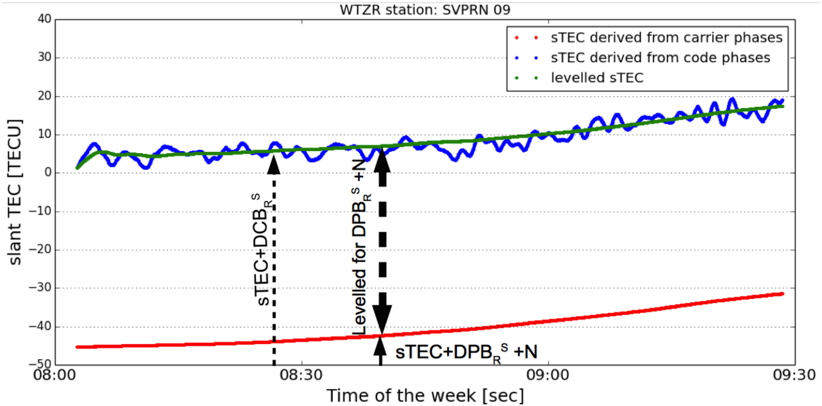

The following basic equation for calibration of DCB has been implemented:

$$sTEC = B' \left(\frac{1}{c} L^s_{GF,R,leveled} - DCB^s_{f1-f2} - DCB^s_{f1-f2,R} \right)$$

Technical University of Berlin

Only observations around local midnight and elevations above 40° have been processed: WTZR March 1, 2015

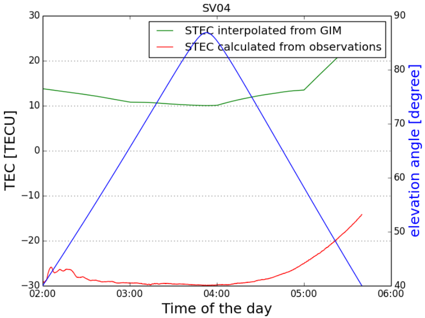

$$B_{R,f1-f2} = 15.420 \pm 0.217$$

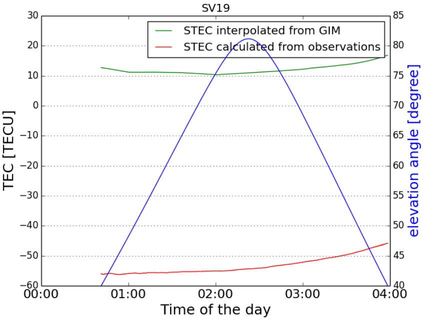

$$B_{R,f1-f2} = 15.880 \pm 0.549$$

Estimation or the receiver DCB

Table : DCB estimation for Wettzell receiver (WTZR - IGS), March 1, 2015

SV	$DCB_{R,f1-f2}$ $[ns]$	RMS $[ns]$	$Local$ $time$	$Duration$
4	15.421	± 0.217	$02:51-06:31$	$03h40m$
11	16.137	± 0.213	$03:23-06:30$	$03h08m$
18	14.854	± 0.288	$00:13-00:51$	$00h38m$
19	15.880	± 0.549	$01:32-04:49$	$03h17m$

$DCB_{WTZR} = 15.573 \pm 0.488$ $[ns]$: estimated

$DCB_{WTZR} = 15.297 \pm 0.043$ $[ns]$: from IONEX

- The estimated DCB is close to the reference one (taken from IONEX).

On-site estimation of the sTEC values

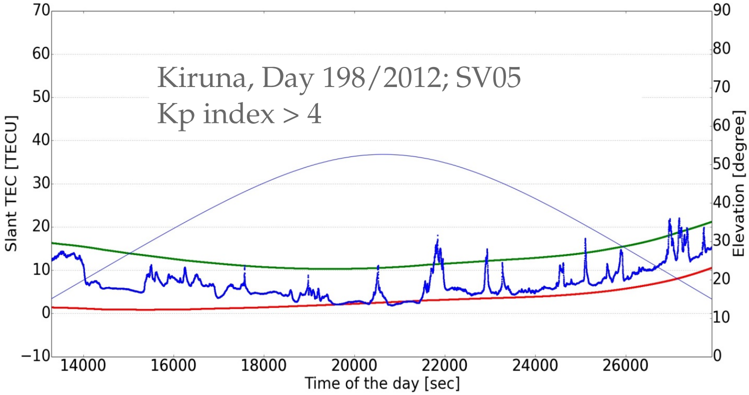

STEC for SV PRN5 derived from: CODE (green), SWACI (red) and calculated with the „TUB-NavSolutions" module (blue)

Rate of Change of TEC

The ROT is calculated as the between epochs difference of TEC [Wanninger,1993]

$$ROT = \frac{sTEC(t_{i+1}) - sTEC(t_1)}{t_{i+1} - t_i} \quad (1)$$

- Calculated from carrier-phase observables
- Carrier-phase cycle slips are controled
- Hardware biases and the carrier-phase ambiguities are canceled

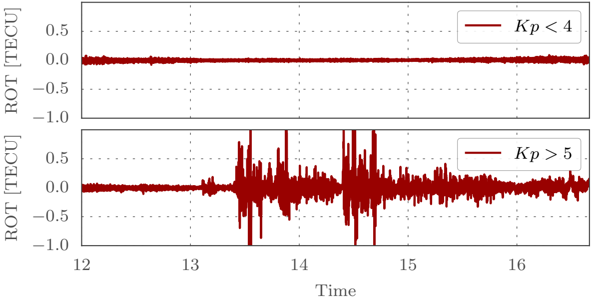

ROT calculated
for Kiruna station (SV15):
16 and 17 March 2015

Signal scintillations

- Ionospheric irregularities diffract radio waves to cause amplitude and phase scintillation of satellites radio signals
- (GPS) signal scintillations are rapid variations in signal's amplitude or phase
- Occur (mainly) at high latitudes (polar cap) and in magnetic equator region

The phase scintillation index σ_ϕ is characterised by standard deviation of the detrended phase $\delta\phi$:

$$\sigma_\phi = \sqrt{E\{\delta\phi^2\} - (E\{\delta\phi\})^2}$$

$\delta\phi$: detrended carrier phase measurements

The amplitude scintillation index $\S_4$ is characterised by standard deviation of the received signal power normalized by its mean as:

$$S_{4,total} = \sqrt{\frac{E\{SI^2\} - (E\{SI\})^2}{(E\{SI\})^2}}$$

SI : signal intensity calculated from **in-phase (I) and quadra-phase (Q)**

Signal scintillations

- Ionospheric irregularities diffract radio waves to cause amplitude and phase scintillation of satellites radio signals
- (GPS) signal scintillations are rapid variations in signal's amplitude or phase
- Occur (mainly) at high latitudes (polar cap) and in magnetic equator region

The phase scintillation index σ_ϕ is characterised by standard deviation of the detrended phase $\delta\phi$:

$$\sigma_\phi = \sqrt{E\{\delta\phi^2\} - (E\{\delta\phi\})^2}$$

$\delta\phi$: detrended carrier phase measurements

The amplitude scintillation index $\S_4$ is characterised by standard deviation of the received signal power normalized by its mean as:

$$S_{4,total} = \sqrt{\frac{E\{SI^2\} - (E\{SI\})^2}{(E\{SI\})^2}}$$

SI : signal intensity calculated from **in-phase (I) and quadra-phase (Q)**

Signal scintillations

- Ionospheric irregularities diffract radio waves to cause amplitude and phase scintillation of satellites radio signals
- (GPS) signal scintillations are rapid variations in signal's amplitude or phase
- Occur (mainly) at high latitudes (polar cap) and in magnetic equator region

The phase scintillation index σ_ϕ is characterised by standard deviation of the detrended phase $\delta\phi$:

$$\sigma_\phi = \sqrt{E\{\delta\phi^2\} - (E\{\delta\phi\})^2}$$

$\delta\phi$: detrended carrier phase measurements

The amplitude scintillation index $\S_4$ is characterised by standard deviation of the received signal power normalized by its mean as:

$$S_{4,total} = \sqrt{\frac{E\{SI^2\} - (E\{SI\})^2}{(E\{SI\})^2}}$$

SI : signal intensity calculated from **in-phase (I) and quadra-phase (Q)**

Amplitude scintillation

The signal power values can be estimated by computing the difference between NBP and WBP the over each bit period N

$$WBP = \sum_{i=1}^{N} I_i^2 + Q_i^2$$: Wide Band Power (WBP)

$$NBP = \left(\sum_{i=1}^{N} I_i^2\right)^2 + \left(\sum_{i=1}^{N} Q_i^2\right)^2$$: Narrow Band Power (NBP)

$$SI \approx NBP - WBP$$: Signal Intensity, signal power

Finally, by removing ambient noise the final amplitude scintillation index can be computed as [Dierendonck et al. 1993]:

$$S_4 = \sqrt{\frac{E\{SI^2\} - (E\{SI\})^2}{(E\{SI\})^2} - \frac{100}{SNR}\left[1 + \frac{500}{19SNR}\right]}$$

ambient noise

Amplitude scintillation

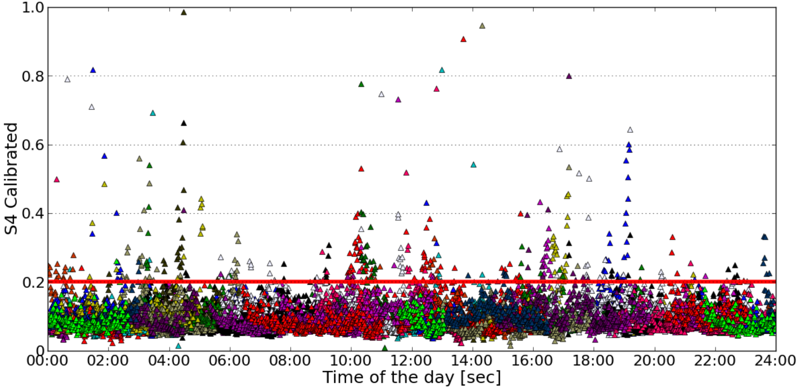

Figure : Amplitude scintillation indices obtained from all visible satellites on 16 July 2012, Kiruna/Sweden

Digital High-Pass Filter Implementation

- A sixth-order Butterworth filter with a 0.1 Hz cutoff frequency
- The filter has a form in the s-plane as: [Dierendonck et al. 1993]

$$Y_i(s) = \frac{s^2}{s^2 + a_i \omega_N s + \omega_N^s} \quad where: \quad f_N = \frac{\omega_n}{2\pi}$$

6th order Butterworth filters as three cascade 2nd-order filters

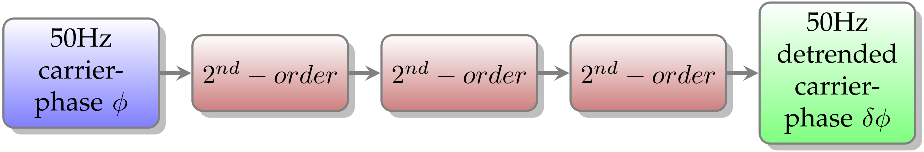

Phase Scintillation

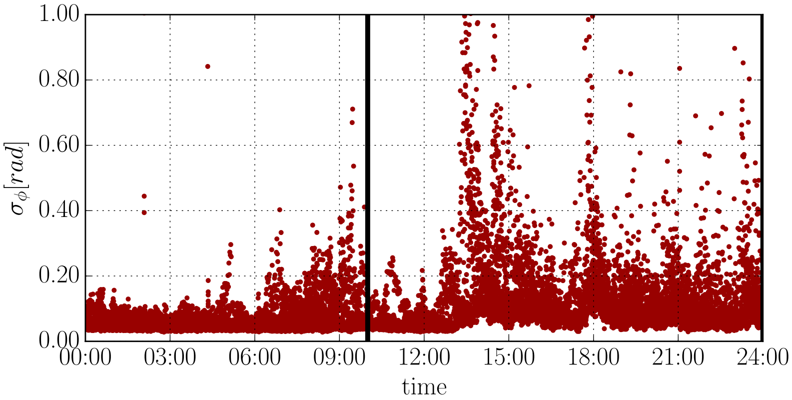

Figure : Phase scintillation indices obtained from all visible satellites on 17 March 2015, Kiruna/Sweden (St. Patrick's day, geomagnetic storm)

IONO-Tools output

Flow diagram of the TUB-software for estimation ionospheric parameters

C, C++, PYTHON

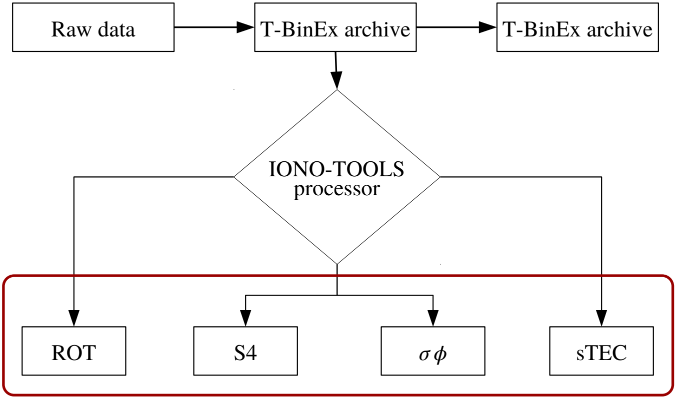

Use of RAIM for Mitigation

In order to monitor reliability of PVT solutions a Receiver Autonomous Integrity Monitoring (RAIM) algorithm is used here

Reliability thresholds are specified by setting values of the two parameters:

- α - Probability of false alarm
- β - Probablitilty of missed detection (risk level)

Those values must be selected very carefully because:

- Setting too large value of α can cause exclusion of a higher number of correct observations.
- Setting too large value of β can cause acception of errornous observations as correct ones.

RAIM algorithm

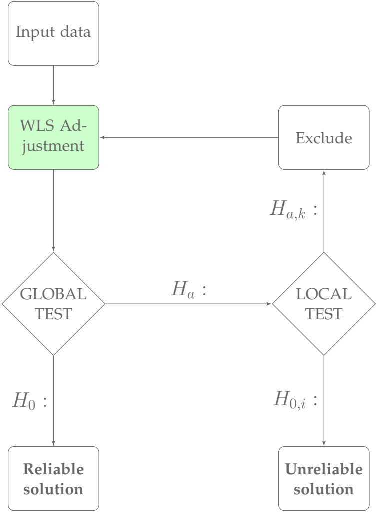

[Walter and Enge1995]

RAIM algorithm

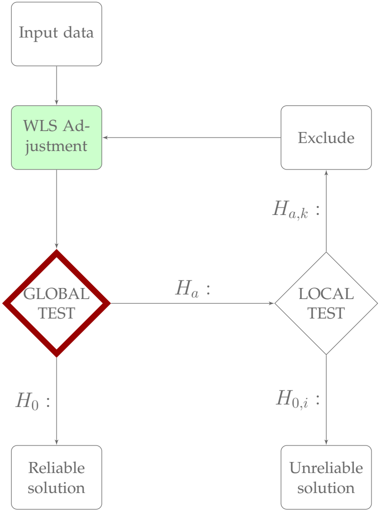

DETECTION: $\Rightarrow$ global test

Null hypothesis: no integrity failure

$H_0 : \hat{v}^T Q^{-1} \hat{v} \leq \chi^2_{1-\alpha,n-p}$

Alternative hypothesis: integrity failure

$H_a : \hat{v}^T Q^{-1} \hat{v} > \chi^2_{1-\alpha,n-p}$

[Walter and Enge1995]

RAIM algorithm

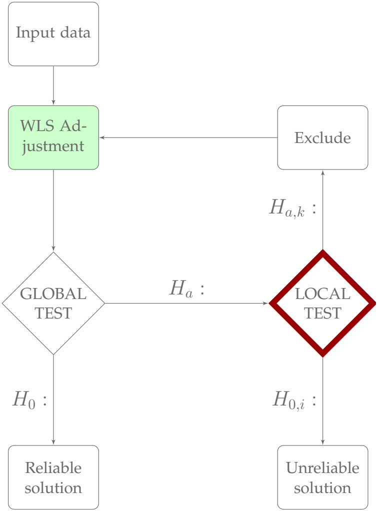

DETECTION: ⇒ global test

Null hypothesis: no integrity failure

$H_0 : \hat{v}^T Q^{-1} \hat{v} \leq \chi^2_{1-\alpha,n-p}$

Alternative hypothesis: integrity failure

$H_a : \hat{v}^T Q^{-1} \hat{v} > \chi^2_{1-\alpha,n-p}$

IDENTIFICATION: ⇒ local test

Null hypothesis: no blunder detect

$H_{0,i} : |Z_k| \leq n_{1-\frac{\alpha_0}{2}}$

Alternative hypothesis: blunder detect

$H_{a,i} : |Z_k| > n_{1-\frac{\alpha_0}{2}}$

[Walter and Enge1995]

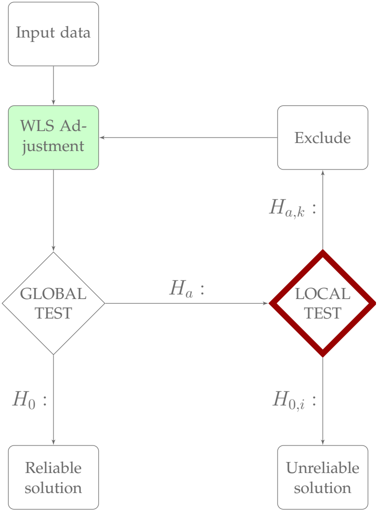

DETECTION: ⇒ global test

Null hypothesis: no integrity failure

$H_0 : \hat{v}^T Q^{-1} \hat{v} \leq \chi^2_{1-\alpha,n-p}$

Alternative hypothesis: integrity failure

$H_a : \hat{v}^T Q^{-1} \hat{v} > \chi^2_{1-\alpha,n-p}$

IDENTIFICATION: ⇒ local test

Null hypothesis: no blunder detect

$H_{0,i} : |Z_k| \leq n_{1-\frac{\alpha_0}{2}}$

Alternative hypothesis: blunder detect

$H_{a,i} : |Z_k| > n_{1-\frac{\alpha_0}{2}}$

EXCLUSION:

$k-th$ observable is an blunder

$H_{a,k} : Z_k \leq Z_i \forall i, \ \wedge \ Z_k > n_{1-\frac{\alpha_0}{2}}$

[Walter and Enge1995]

RAIM algorithm

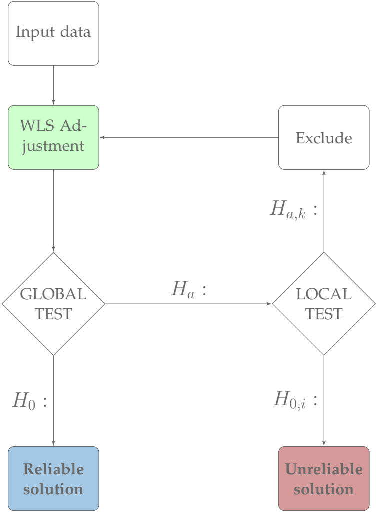

DETECTION: $\Rightarrow$ global test

Null hypothesis: no integrity failure

$H_0 : \hat{v}^T Q^{-1} \hat{v} \leq \chi^2_{1-\alpha,n-p}$

Alternative hypothesis: integrity failure

$H_a : \hat{v}^T Q^{-1} \hat{v} > \chi^2_{1-\alpha,n-p}$

IDENTIFICATION: $\Rightarrow$ local test

Null hypothesis: no blunder detect

$H_{0,i} : |Z_k| \leq n_{1-\frac{\alpha_0}{2}}$

Alternative hypothesis: blunder detect

$H_{a,i} : |Z_k| > n_{1-\frac{\alpha_0}{2}}$

EXCLUSION:

$k-th$ observable is an blunder

$H_{a,k} : Z_k \leq Z_i \forall i, \ \wedge \ Z_k > n_{1-\frac{\alpha_0}{2}}$

[Walter and Enge1995]

Selected Stochastic Models

Traditional stochastic models

- Elevation dependent model [Rothacher et al., 1998]:

$$w(el) = sin^2(el)$$

- C/N0 dependent model ($SIGMA - \epsilon$) [Hartinger and Brunner, 1999]:

$$w(C/N0) = 1/(C_i exp^{-(\frac{C/N0}{10})})$$

$w(\cdot)$: weight of undifferenced observation
$C/N0$: phase scintillation index
el : satellite elevation angle
C_i : empirical constant

Investigated Stochastic Models

The uncorrelated behaviour of the scintillation and satellite elevation angle implies the unrealistic assumption made by elevation-dependent weighting models

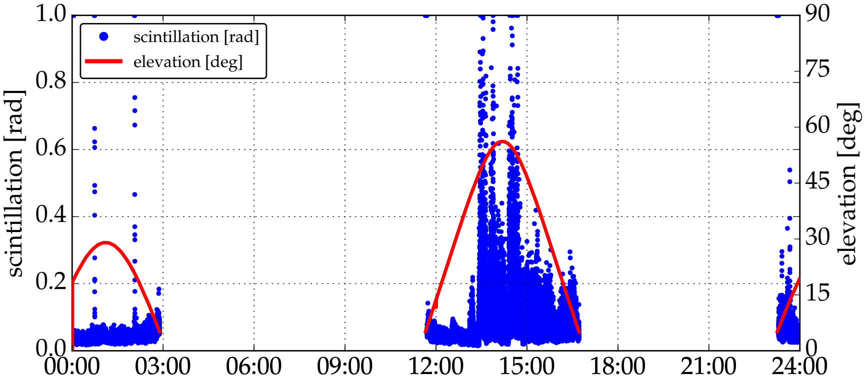

Figure : Phase scintillation and satellite elevation angle measured at station Kiruna/Sweden (March 17th, 2015) for satellite PRN 15

Investigated Stochastic Models

Proposed stochastic models

- Scintillation dependent model:

$$w(S_{idx}) = 1 + a\exp^{-S_{idx}}$$

- Scintillation & Elevation dependent model:

$$w(S_{idx}, el) = 1 + sin^2(el) \cdot \exp^{-S_{idx}}$$

$w(\cdot)$: weight of undifferenced observation
S_{idx} : phase scintillation index
el : satellite elevation angle
a : empirical constant

Investigated Stochastic Models - Weights

Technical University of Berlin

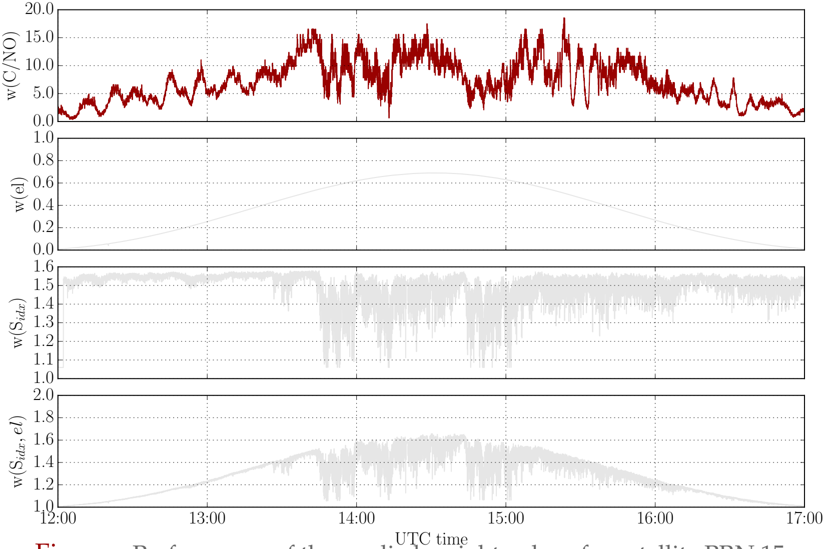

Figure : Performance of the applied weight values for satellite PRN 15

Investigated Stochastic Models - Weights

Technical University of Berlin

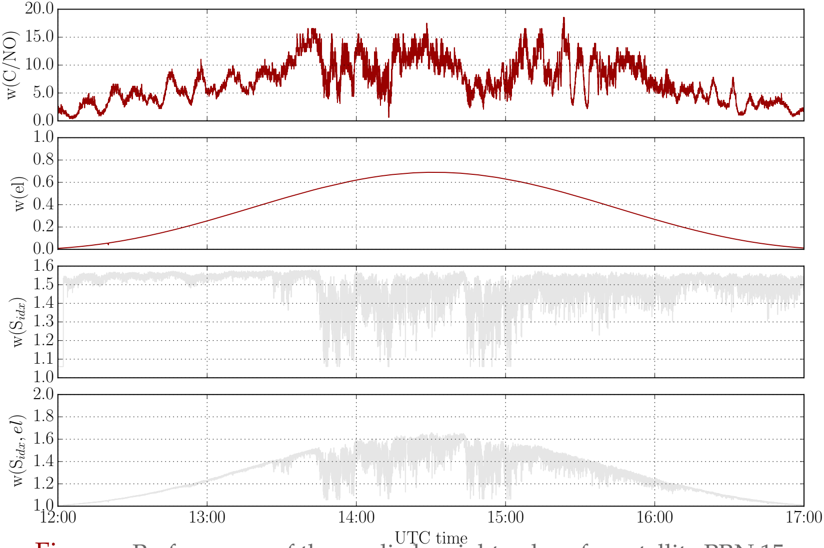

Figure : Performance of the applied weight values for satellite PRN 15

Investigated Stochastic Models - Weights

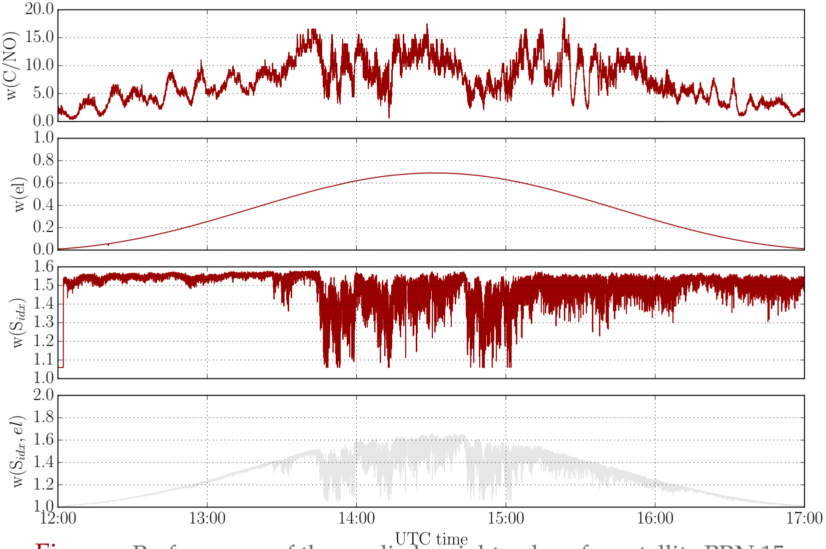

Figure : Performance of the applied weight values for satellite PRN 15

Investigated Stochastic Models - Weights

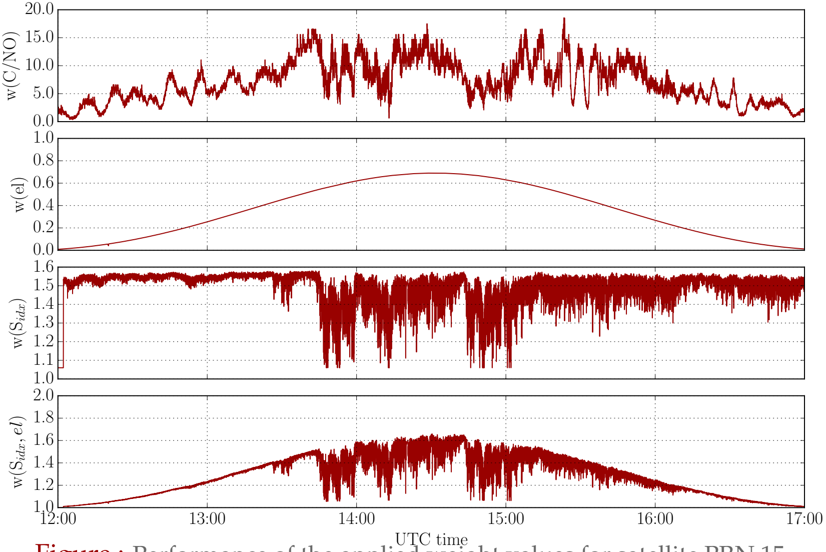

Figure : Performance of the applied weight values for satellite PRN 15

Experimental Setup

DLR

Technical University of Berlin

Parameters	Setup
Observables	
Receiver site location	Kiruna/Sweden: 67.84°N, 20.41°E
Time of observation	March 17, 2015 (DOY 076)
Type of observables: positioning	GPS C/A code-phase (1Hz)
Type of observables: scintillation	GPS L1 carrier-phase (50Hz)
Cut-off angle	5 °
Positioning model	
Observational model	Undifferenced (SPP)
Stochastic model	Variances along the diagonal
A priori models	
Tropospheric model	Saastamonien
Ionospheric model	Klobuchar
RAIM settings	
Probability of false alarm	5%
Probablitilty of missed detection	20%

Numerical Results

Technical University of Berlin

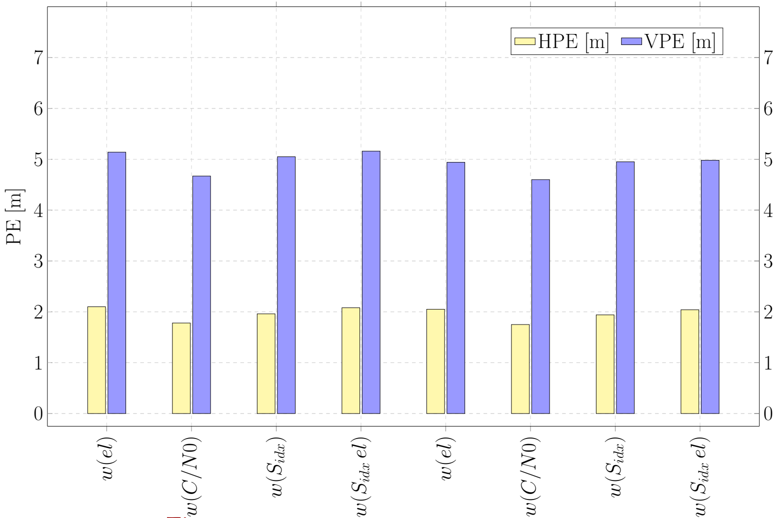

Figure : Horizontal and Vertical RMS [m]

Numerical Results - without RAIM

Technical University of Berlin

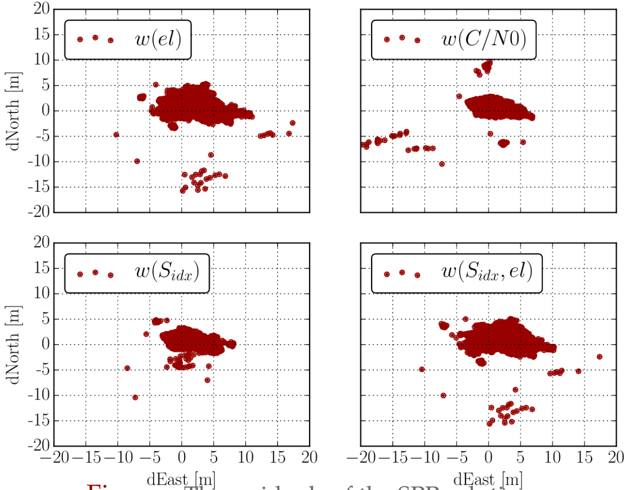

Figure : The residuals of the SPP solution

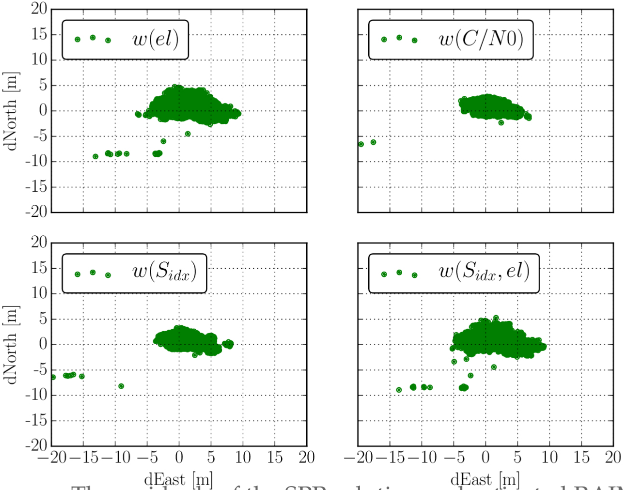

Figure : The residuals of the SPP solution and activated RAIM

Numerical Results

Number of unreliable solutions and rejected observations (WLS+RAIM)

Stochastic model	# of unreliable solutions	# of rejected observations
Elevation Angle	220 (0.44%)	2378
C/N0	856 (1.70%)	1821
Scintillation	129 (0.26%)	979
Scintillation & Elev. Angle	188 (0.37%)	1821

Summary and Future Activities

- CONCLUSION
  - Usage of the scintillation-based stochastic model in the RAIM can enhance reliability of GPS based positoning under presence of ionospheric local disturbances.
- FUTURE ACTIVITIES
  - Further analysis will be addressed on carrier-phase

Summary and Future Activities

- CONCLUSION
  - Usage of the scintillation-based stochastic model in the RAIM can enhance reliability of GPS based positoning under presence of ionospheric local disturbances.
- FUTURE ACTIVITIES
  - Further analysis will be addressed on carrier-phase

Thank you for your attention

M.Sc.Eng. Kinga Węzka kinga.wezka@tu-berlin.de

ACKNOWLEDGMENT

- The first author has been supported by the German Federal Ministry of Education and Research (BMBF) listed under the support code 16N036426
- Additionally, the authors gratefully acknowledge the contribution of the Department of Nautical Systems of the German Aerospace Centre for providing the necessary GNSS data, with which the present study has been performed

References I

Technical University of Berlin

- M. Aquino, J. F. G. Monico, A. Dodson, H.; Marques, G. D.,Franceschi, L. Alfonsi, V. Romano and M. Andreotti: *"Improving the GNSS positioning stochastic model in the presence of ionospheric scintillation"*; Journal of Geodesy, Vol. 83, pp. 953-966, 2009,
- J. Aarons,: *"Global Morphology of Ionospheric Scintillations"*; in proceedings of the IEEE, Vol.. 7O, No. 4, 1982
- Baarda, W. : *A testing procedure for use in geodetic networks*; Delft, Kanaalweg 4, Rijkscommissie voor Geodesie 2(5), 1968.
- J. Bartels,: *"The technique of scaling indices K and Q of geomagnetic activity"*; Annals of the International Geophysical, Year 4, pp. 215-226,1957
- S. Basu, K. Groves, S. Basu and P. Sultan,: *"Specification and forecasting of scintillations in communication/navigation links: current status and future plans"*; Journal of Atmospheric and Solar-Terrestrial Physics, Vol. 64, pp. 1745-1754, 2002
- R. Dach, U. Hugentobler, P. Fridez and Meindl, M. *„Bernese GPS Software Version 5.0"*; 2005
- A.J.V. Dierendonck, J.A. Klobuchar and Q. Hua, *"Ionospheric Scintillation Monitoring Using Commercial Single Frequency C/A Code Receivers"*; ION GPS-93, 1333, The Institute of Navigation, Arlington,1993

- P.H. Doherty, S.H. Delay, C.E. Valladares and J. A. Klobuchar, *"Ionospheric Scintillation Effects on GPS in the Equatorial and Auroral Regions"*; Journal of The Institute of Navigation, Vol. 50, 2003
- Hartinger, H. and Brunner, F.: *Variances of GPS phase observations: The SIGMA model*; GPS Solutions 2(4), 35–43, 1999
- Parkinson, B. and Axelrad, P. : *Autonomous GPS integrity monitoring using the pseudorange residual* ; Journal of The Institute of Navigation 35(2), 255–274, 1988
- Parkinson, B. and Axelrad, P. : *A basis for the development of operational algorithms for simplified GPS integrity checking*; in : Institute of Navigation, Technical Meeting, 1st, Colorado Springs, CO, Sept. 21-25, 1987, Proceedings (A88-37376 15-04). Washington, DC, Institute of Navigation, p. 269-276, 1987
- M. Rothacher, T.A. Springer, S. Schaer and G. Beutler, *"Processing Strategies for Regional GPS Networks"*; Proceedings of the IAG General Assembly (ed. Brunner, F.K), Rio de Janeiro, Brazil, 3-9 September 1997, IAG Symposia, 93-100, Springer Verlag, Berlin/Heidelberg/New York, 1998
- T. Walter and P. Enge, *"Weighted RAIM for Precision Approach"*; Stanford University, 1995

Numerical Results

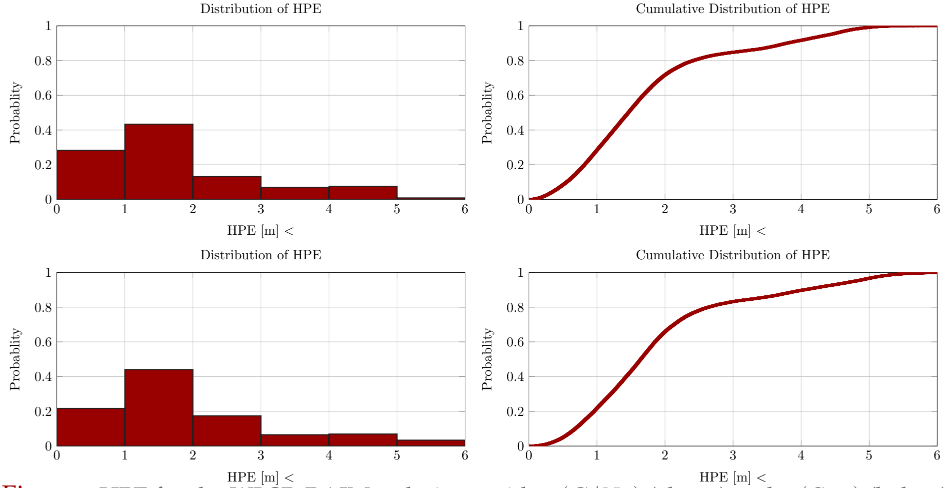

Figure : HPE for the WLSR-RAIM technique with $w(C/N0)$ (above) and $w(S_{idx})$ (below)

Numerical Results

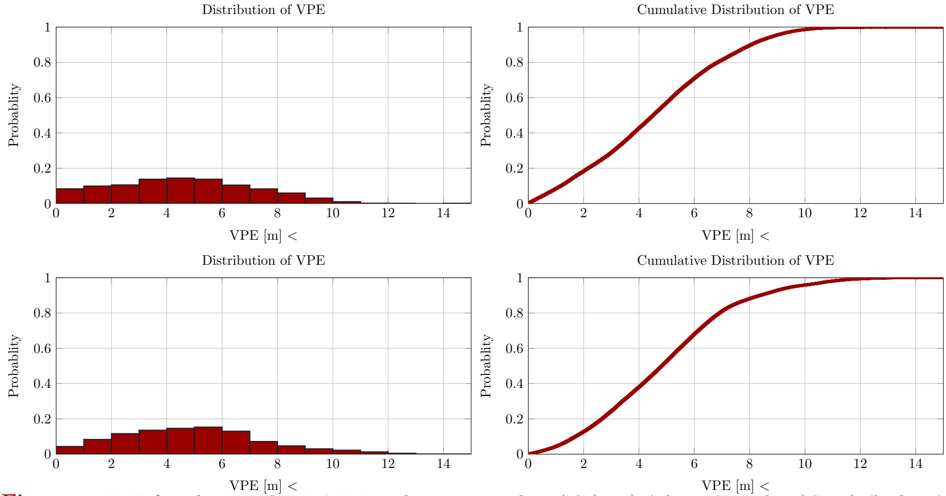

Figure : VPE for the WLSR-RAIM technique with $w(C/N0)$ (above) and $w(S_{idx})$ (below)

Receiver DCB taken from the CODE

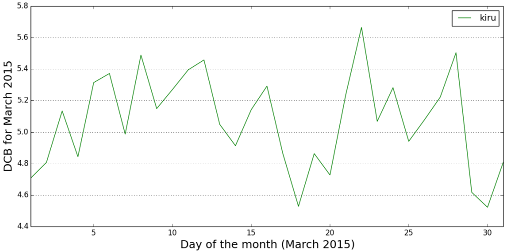

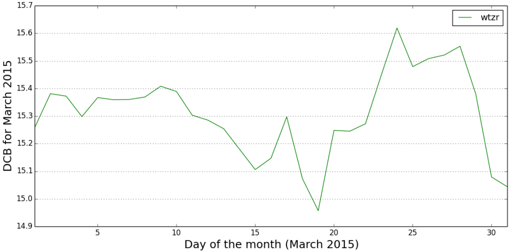

Flow diagram of the TUB-software for estimation of: sTEC, and receiver DCB

C, C++, PYTHON